Ruthenium on Alkali-Exfoliated $Ti_3(Al_{0.8}Sn_{0.2})C_2$ MAX Phase Catalyses Reduction of 4-Nitroaniline with Ammonia Borane

Thierry K. Slot,[a] Paula Oulego,[b] Zdeněk Sofer,[c] Yuelei Bai,[d] Gadi Rothenberg,[a] and N. Raveendran Shiju*[a]

MAX phases are gaining increased interest in catalysis, typically for high-temperature applications. They can also be delaminated into 2D-structures, so-called MXenes, enabling better accessibility and the tuning of active site surroundings. Here we present an analogous yet different approach, using an alkaline treatment to prepare a $Ti_3(Al_{0.8}Sn_{0.2})C_2$ MAX phase derivative, with an open, disordered structure. This new material, which is missing most of the larger interlayer spacing, is a good support for ruthenium particles (1.6 nm diameter). Ru on disordered MAX phase catalyses both ammonia borane hydrolysis (TOF = 582 min^{-1}, 30 °C) and the reduction of 4-nitroaniline (TOF = 13 min^{-1}, 45 °C). Using the former as a benchmark reaction, we show that the open disordered structure of the support promotes catalytic activity. The boost in reactivity is related to a metal-support interaction, improving the activity of metallic ruthenium. We also show here, for the first time, that supported Ru is a good catalyst for reducing nitroaniline with ammonia borane. Overall, our results reveal that disordered MAX-derivatives are promising as catalyst supports, owing to their potential for tuning the electronic properties at the metal active sites.

Introduction

Heterogeneous catalysis occurs at active sites, but in many cases the support itself also plays an important role. This is especially true for MAX phases, a novel class of laminar materials with the formula $M_{n+1}AX_n$, where M is an early transition metal, A is an element in group 13 or 14, and X is either carbon or nitrogen.[1] They are stable at extreme conditions, making them very useful for high-temperature reactions, such as oxidative dehydrogenation and dry reforming.[2,3] For low-temperature reactions, we want to open up the MAX phase structure, improving accessibility. One way to do this is by extracting the 'A' layers, resulting in layered transition metal carbides or nitrides, so-called MXenes.[2,4,5] These are noted as $M_{n+1}X_nT_x$, where T stands for a terminating functional group that depends on the delamination conditions.[4,6,7] The chemistry of MAX phases and MXenes was studied extensively in the past few years, especially for electrocatalysis,[6,8–12] yet their thermo-catalytic applications are less known.[13]

MAX phases can be delaminated into MXenes thanks to the weaker M–A bonds. Most of the delamination methods use HF or fluorides.[14–19] The resulting fluor-based MXenes are sensitive to oxidation.[20–23] Recently, less hazardous delamination methods were developed using alkaline treatment.[24] The literature describes a variety of treatments, ranging from low NaOH concentrations all the way to molten NaOH.[25–28] Such etching dissolves the aluminium between the titanium carbide layers, causing delamination. Zhang *et al.* reported etching and exfoliation of Ti_3AlC_2 in alkaline conditions, obtaining delaminated MAX phases, also known as $Ti_3C_2T_x$ MXenes.[24] They found that successful exfoliation depends on temperature and NaOH concentration, producing MXenes rich in oxide or hydroxyl terminal groups.

Partially delaminated MXenes (obtained by HF treatment) can be delaminated further using bases such as NaOH, KOH and LiOH.[24,29–32] This treatment gives a composite material with needle-like titanate structures on top of the MXene layer.[33] The exact composition of these structures is unknown. For example, treating $Ti_3C_2T_x$ MXene with sodium hydroxide

[a] Dr. T. K. Slot, Prof. G. Rothenberg, Dr. N. Raveendran Shiju
Van't Hoff Institute for Molecular Sciences
University of Amsterdam
Science Park 904
1098 XH Amsterdam (The Netherlands)
E-mail: n.r.shiju@uva.nl
[b] Dr. P. Oulego
Department of Chemical and Environmental Engineering
University of Oviedo
c/Julián Clavería 8
33006 Oviedo, Asturias (Spain)
[c] Prof. Z. Sofer
Department of Inorganic Chemistry
University of Chemistry and Technology Prague
Technická 5
166 28 Prague 6 (Czech Republic)
[d] Dr. Y. Bai
National Key Laboratory of Science and Technology on Advanced Composites in Special Environments and Center for Composite Materials and Structures
Harbin Institute of Technology
Harbin 150080 (P. R. China)

Supporting information for this article is available on the WWW under https://doi.org/10.1002/cctc.202100158

gives $NaTi_{1.5}O_{8.3}$,[33] $Na_2Ti_3O_7$,[30,33] and $NaTi_8O_{13}/NaTiO_2$.[31] Sodium titanates (NTOs) are useful as anode materials in electrocatalysis,[31,34] but in delamination they are unwanted impurities.

Here we study the potential of an alkaline-etched MAX phase, $Ti_3(Al_{0.8}Sn_{0.2})C_2$, as a support for metal nanoparticles.[35] Taking ammonia borane hydrolysis and the reduction of 4-nitroaniline as test reactions, we show that this disordered MAX phase enhances the activity and stability of supported ruthenium nanoparticles. Its structure is more open, enabling a better electronic interaction with ruthenium, thereby boosting catalytic activity. Our results show how the surface-particle interactions of Ru on NaOH-treated MXene influences both the hydrogen generation and reduction reactions. To the best of our knowledge, this is also the first report of a Ru-catalysed hydrogenation of 4-nitroaniline (4NA) with ammonia borane (AB).

Results and discussion

First, we synthesized the $Ti_3(Al_{0.8}Sn_{0.2})C_2$ MAX phase (herein TASC) by heating Ti, Al and, Sn and TiC in a 1:1:0.2:1.9 ratio (see experimental section for details). We then opened this structure by NaOH treatment at 200, 275 and 350 °C for 20 h. The material was then impregnated with ruthenium particles using the double solvent method.[36] The catalysts were then tested in ammonia borane hydrolysis (Eq. 1) using our bubble counter to monitor hydrogen production.[37] We know that the reactivity for H_2 generation and reduction reactions often go hand in hand, making AB hydrolysis a nice way to screen catalysts for both reactions.[38,39] The bubble counter setup quantifies the produced H_2 volume and by ramping a catalytic experiment from 20 °C to 80 °C at 2 °C min^{-1}, we can get the relationship between temperature and TOF.[37] TOF was compared at 30 °C, since at that temperature, the conversion of each reaction is still low (generally less than 10%) making the observed rate a close approximation of the initial rate. Isothermal control experiments verified the rate order in ammonia borane to be 0.18 (Figure S13), illustrating the small influence of AB concentration on the rate. The TOF observed at higher temperatures might be slightly underestimated because of reduced AB concentrations.

$$NH_3BH_3 + 4H_2O \xrightarrow[20\text{ - }85°C,\ 45\text{ min}]{\text{Ru/TASC-NaOH}} \overset{\oplus}{NH_4} + \overset{\ominus}{B(OH)_4} + 3H_2 \quad (1)$$

Turnover frequency (TOF) values were calculated by the rate of gas formation (mol_{H2}/mol_{Ru}), assuming all impregnated Ru is available for catalysis (in practice, the TOF values per available Ru atom could be higher). All NaOH treatments of the TASC enhanced the activity of the ruthenium when compared to Ru on untreated TASC (64 min^{-1}, Figure 1). The materials before impregnation (without Ru) were inactive. Treatment at 275 °C gave the highest TOF (250 min^{-1} at 30 °C), a four-fold improvement over the untreated sample. This temperature is slightly above those used by Li *et al.*[24] Volume-time data shows the reaction completes with generation of 3 equivalents of hydrogen (Figure S11).

This improved activity prompted us to further study the structure of the materials. During treatments at temperatures 200 °C, 275 °C and 350 °C, the volume of the material increased by 2×, 3–4× and 10×, respectively. Using scanning electron microscopy (SEM) we identified ribbon-like structures emerging from the basal plane of the MAX phase (*cf.* Figures 2a/c). At 200 °C, small crystalline structures appear (Figure 2b), which can be attributed to NaOH crystals. At 275 °C, long nanoribbons appear with a thickness of 15–50 nm and an average width of 180 nm (50–400 nm, see Figure 2c). We expect these ribbons to be either MXene or some form of titanate or aluminate.[31,33] X-ray diffraction (XRD) showed no other crystalline phase besides the MAX phase, nor a broad background that could be attributed to amorphous material (Figure S1). At 275 °C, the MAX signals at 9° and 18° related to the interlayer ordering of 002 and 004 disappeared while the other MAX signals

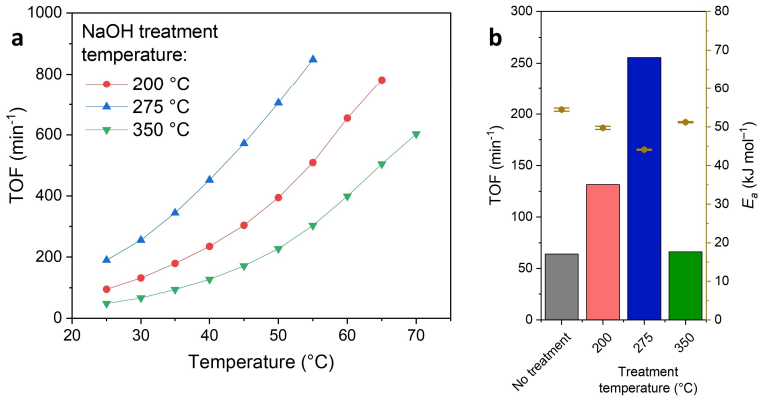

Figure 1. (**a**) Catalytic data for 1 wt% Ru catalysts prepared from the NaOH-treated materials at different temperatures. Each point is a window average of at least 20 measurements. (**b**) Bar graph of TOF at 30 °C with the apparent activation energy (E_a) for each material. Error bars represent the standard deviation in E_a, as derived from a linear fit of each Arrhenius plot based on 3000 measured data points.

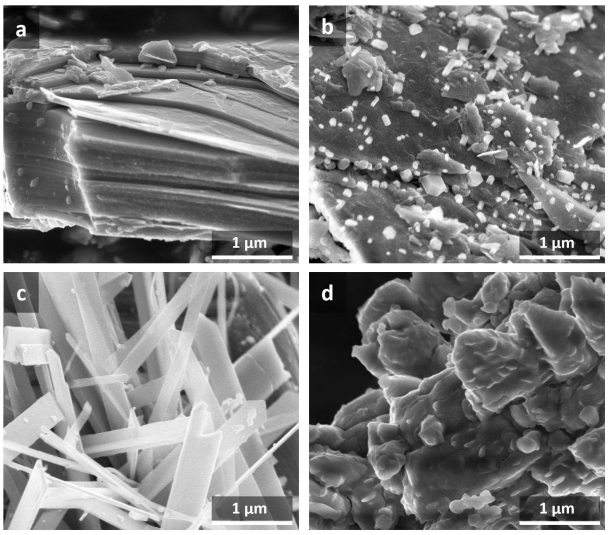

Figure 2. Scanning electron micrographs of (**a**) pristine TASC MAX phase, TASC MAX phase after NaOH treatment at temperatures: (**b**) 200 °C, (**c**) 275 °C, and (**d**) 350° for 20 h.

remained. This indicates that the ordering in these directions is lost by interlayer separation. The XRD data suggests that the material contains a disordered MAX bulk phase with partially exfoliated MXene ribbons on its surface.

The NaOH reacts with the Al layers of the MAX phase, starting with the exposed Al at the sides, then moving inwards. During this reaction, $Al(OH)_4^-$ and hydrogen gas form. We hypothesize that the combination of aluminium hydration on a microscopic level and gas evolution on a macroscopic level push the MAX layers apart, snapping off the MXene ribbons in the process. The NaOH treatment leaves more tin exposed on the surface (*cf.* entries 1 and 2, Table 1), and tin does not catalyse AB hydrolysis (see the line marked "no cat" in Figure 3a). X-ray photoelectron spectroscopy (XPS) elemental mapping confirmed the loss of aluminium (see Table 1, entry 1) and showed very low levels of sodium (1.7 at%) on the surface after treatment. This means that these structures are not sodium titanate nor any other titanate/aluminate. Zhang *et al.* suggests NaOH treatment requires >20 M concentrations to suppress any NTO formation.[24] We did not observe NTO formation at 4 M concentrations. Low NaOH concentrations have the advantage that less sodium is retained by the material (1.7 at%, see Table 1) compared to 6.3 at% reported previously.[24] Using SEM-EDS elemental mapping, we learned that the surface of the needles contains Ti, C, and O, suggesting a MXene or oxidized MXene structure (Figure S14).

Under hydrothermal conditions, the $Ti_3C_2T_x$ MXene can form crystalline TiO_2 structures.[21,40–42] However, the XRD data shows neither anatase nor rutile titania. This is because our method does not introduce any electron-withdrawing fluor groups. These make the titanium atoms vulnerable to nucleophilic attack and thus TiO_2 formation. Additionally, the alkaline environment halts the decomposition of NTO structures into TiO_2 and water, which typically occurs under acidic conditions. FTIR spectra (data not shown) show the presence of –OH and –O groups, so we assume the MXene surface is covered mainly with oxygen functionalities. Raman spectroscopy shows two new signals at 201 and 273 cm^{-1} compared to pristine TASC (Figure S2). In the samples treated at 275 and 350 °C the D and G bands at 1350 and 1575 cm^{-1} (characteristic for graphitic layers) are absent. The sample treated at 350 °C shows two faint signals at 781 and 868 cm^{-1} that correspond to titanate structures.[27] This, combined with the absence of any TASC signals and/or other sharp signals in XRD (Figure S1, top curve), implies that most of the TASC has converted into amorphous titanate(s). Throughout the different treatment temperatures, the signals from MAX phase at 391 and 626 cm^{-1} (corresponding to titanium oxycarbides, TiO_xC_y) are observerd. This suggests there is no significant change in the surface groups and the structures connecting them.[43] Signals from anatase and rutile TiO_2 appear at similar locations, although the most characteristic signals for anatase E_g at 145 cm^{-1} and E_g/A_{1g} at 640/611 cm^{-1} are absent.[44–46] We also see a signal at 137 cm^{-1} which cannot be attributed to simple TiO_2. This signal is probably caused by an oxycarbide species. From XPS quantification we derived the Ti:O:C element ratios as 1:3:1 (Table 1, entry 1), excluding adsorbed water in the calculation. This supports our hypothesis that the surface is covered with oxycarbide species.

We compared the NaOH-treated materials to five other support materials that are similar in structure or composition: TASC MAX phase, anatase TiO_2, MXene prepared using HF, oxidized MXene and alumina (Figures 3a/c and S12). The NaOH-treated materials are superior in the hydrolysis of ammonia borane, giving turnover frequencies of 315 and 582 min^{-1} for the samples containing 1 wt% and 0.4 wt% Ru, respectively. This TOF is amongst the top quartile of reported TOFs for

Table 1. Overview of chemical composition of the surface by XPS analysis and total Ru content by ICP-MS.[a]

#	Method: Material	ICP-MS[a] Ru[a] [wt%]	X-ray Photoelectron spectroscopy[b] [at%] Ru 3d[c]	Sn 3d	C 1s[d]	O 1s	Ti 2p[e]	Al 2s	F 1s	Na 1s
1	Ru/TASC-NaOH	0.355[f]	5.9	0.57	14	65	13	0.0	–	1.7
2	Ru/TASC	0.38[f]	3.2	0.34	10	61	9.1	15	–	1.1
3	Ru/MXene	0.42	2.6	–	34	37	12	4.1	10	0.5
4	Ru/TiO_2 anatase	0.39	3.2	–	23	49	24	–	–	1.3

[a] Triplicate experiments, standard deviation <0.01 wt%. [b] Based on region scans using the deconvoluted adventitious carbon (284.8 eV) signal as internal standard. [c] Partially overlapping with C 1s. [d] All C 1s signals excluding adventitious carbon. [e] Overlapping with Ru 3p signal. [f] Based on quadruple experiments.

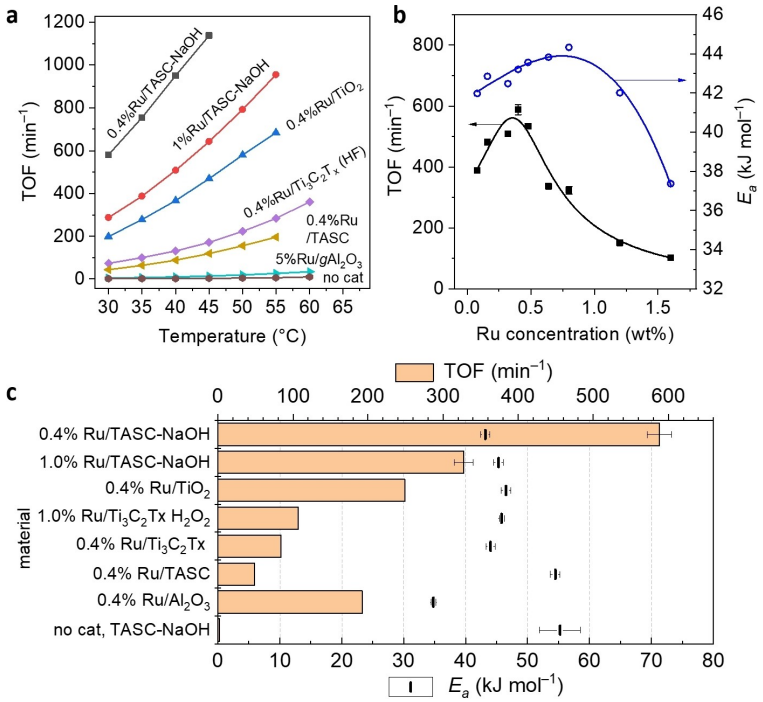

Figure 3. Catalytic data for (**a**) TOF at different temperatures, (**b**) Various concentrations of Ru/TASC-NaOH catalysts versus TOF (left axis), and apparent activation energy (E_a, right axis). (**c**) TOF values (at 30 °C) and activation energies for various ruthenium-impregnated materials in the hydrolysis of ammonia borane. Error bars depict standard deviation.

ammonia borane hydrolysis (Table S2). However, most literature catalysts were measured at 25 °C instead of 30 °C in our work. We chose 30 °C because our 2 °C min ramp needs to heat roughly 5 °C to stabilize, making 30 °C the lowest temperature that produces an accurate TOF. Ru-catalysed hydrolysis of AB generally gives 3 equivalents of H_2.[47–58] From earlier work, we know that NaOH itself enhances the hydrolysis of ammonia borane by about 30 %.[59] Our materials were rinsed extensively with deionized water to avoid NaOH carry-over. A series of control experiments with added NaOH showed that the TOFs increased by 5–25 %.

Because of the large difference between the sample prepared with 0.4 wt% Ru and 1 wt% Ru, we decided to study the effect of Ru loading on the catalytic activity. We impregnated the NaOH-treated material with 0.08, 0.16, 0.32, 0.40, 0.48, 0.64, 0.80, 1.2 and 1.6 wt% ruthenium. We observed an optimum at around 0.4 wt%, where the highest turnover frequencies were observed (Figure 3b). Our bubble counting device can generate Arrhenius plots with hundreds of data points from a single experiment. This allows us to detect small differences (<1 kJ/mol) in apparent activation energy.[37] The best performing catalyst had an apparent activation energy of 43 kJ/mol and contained 0.4 wt% ruthenium. This activation energy differs from that of Ru/TASC and commercial Ru/Al_2O_3 (Figure 3c). The apparent activation energy correlates with the catalytic activity. This means that the reactive species in these catalysts exhibit the same rate-determining step and mechanism for AB hydrolysis. The apparent activation energy increases from 0.1 wt% loading to 1 wt% loading, likely because of a change in Ru particle size. At ruthenium loadings >1 wt%, the apparent activation energy decreases rapidly. This may be caused by the low surface area (3.2 $m^2 g^{-1}$) of the TASC-NaOH material, reducing the dispersion of ruthenium at higher loadings.[24]

Transmission electron microscopy and scanning transmission electron microscopy using high-angle annular dark-field (STEM-HAADF) imaging revealed that the Ru particles are well dispersed on the needle-like structures with an average size of 1.6 nm (Figure 4c, d, the Ru particle size distribution for Ru/TASC-NaOH is included in Figure S9). The particles are close together, yet still apart. We think the Sn at the surface of the needle-like structures of the TASC-NaOH, helps to anchor and grow the Ru nanoparticles.

Our catalyst screening gave three catalysts with 0.4 wt% Ru that were most active: Ru/TASC-NaOH, Ru/TASC and Ru/TiO_2. Though TASC-NaOH has a more open structure than TASC, its surface area (3.2 $m^2 g^{-1}$) is still much lower than TiO_2 catalyst (226 $m^2 g^{-1}$, Figure S7). Yet Ru/TASC-NaOH and Ru/TASC are more active than Ru/TiO_2 (Figure 3a). We then tested the catalysts in the reduction of 4-nitroaniline using ammonia borane as the reductant (Figure 5). Without ruthenium there was no reaction. The three best catalysts for AB hydrolysis also performed well in the hydrogenation of 4-nitroaniline, giving a TOF value of 13 min^{-1} for the Ru/TASC-NaOH catalyst at 30 °C. This was the best catalyst, followed by Ru/TASC and Ru/TiO_2 (Figure 5c). Commercial Ru/C and $Ru/Ti_3C_2T_x$ (which was exfoliated using the common HF method) showed almost zero to no reactivity. To compare our TOF values to literature results,

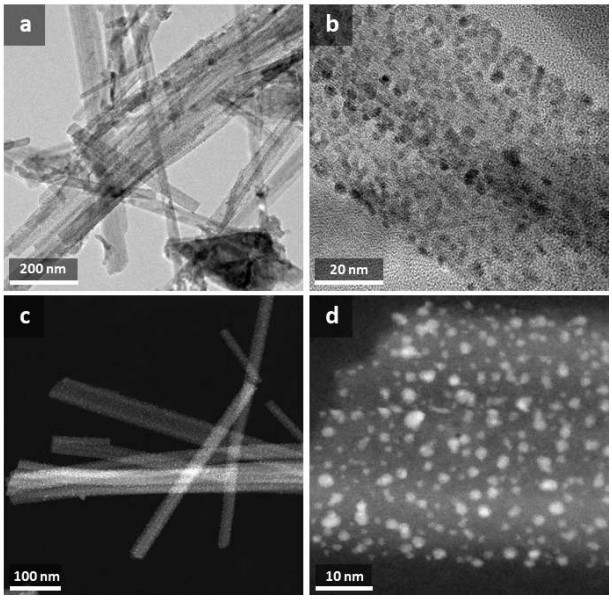

Figure 4. (**a**, **b**) Transmission electron micrographs of Ru/TASC-NaOH and (**c**, **d**) STEM-HAADF images of the same catalyst.

we also ran experiments at 25 °C; Ru/TASC-NaOH, Ru/TASC and Ru/TiO_2 gave TOF values of 7.1, 6.6, and 3.9 min^{-1}, respectively. Literature TOF values range from 1.25 min^{-1} to 97 min^{-1} (Table 2). Our catalyst performs well, and often better than most noble metal catalysts. We mainly used a reaction temperature of 45 °C in further experiments because this reduced the amount of scattering by bubbles in our UV/Vis analysis setup. Ru/TASC-NaOH remained stable for 6 reaction cycles, however Ru/TASC showed slight degradation after 6 cycles (Figure S10). Probably, some of the Ru particles are lost because they adhere less to the MAX phase support.

The fact that the catalysts perform well in both reactions was unexpected, because a catalyst that performs well in H_2 generation (from AB) would leave less AB for reaction with 4-nitroaniline. As such, the mechanisms of both reactions may be similar. Hydrogenation of 4-nitroaniline using boranes generally follow either a tandem reduction pathway,[65–70] or a transfer hydrogenation pathway.[62,71–73] A tandem hydrogenation first produces hydrogen, which is then used as reductant in an ensuing reaction.[38,66,74] Transfer hydrogenation starts with B–H bond cleavage, to give an [M]–H active species. This species rapidly reduces nitro arenes into the corresponding N-aryl hydroxylamines, which are reduced further into aryl amines using NH_3BH_3.[63] Ammonia borane hydrolysis is believed to proceed through a Langmuir-Hinshelwood type mechanism with O–H bond cleavage as the rate-determining step.[75,76] However, the exact reactive species is unknown.[77–84] Ammonia borane likely first adsorbs on the metal surface after which one B–H bond dissociates, forming NH_3BH_2* and H* (analogous to the previous mechanism).

Then, water adsorbs and dissociates into OH*, and a H^+/e^- pair. This H^+/e^- pair combines with H* to form hydrogen, and

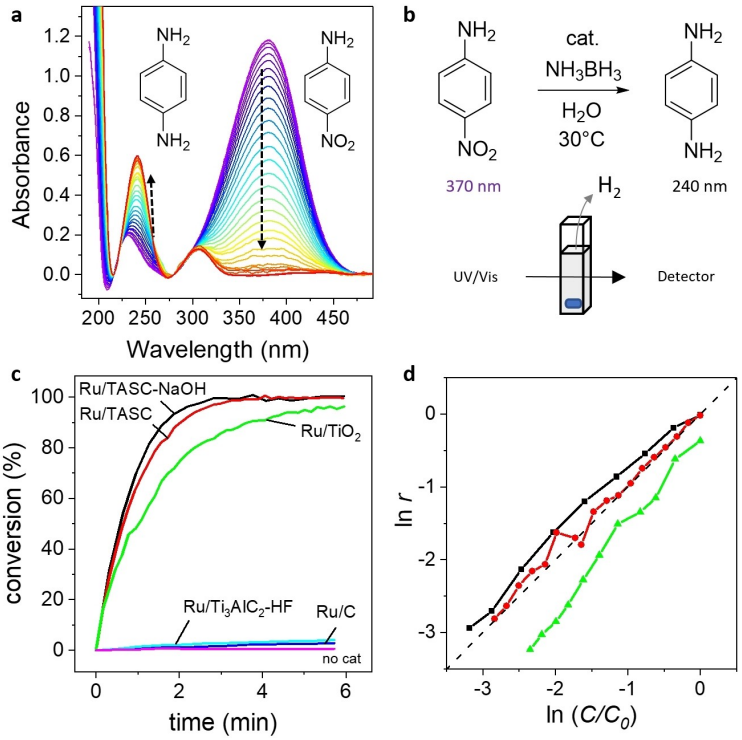

Figure 5. (**a**) Background-corrected UV/Vis spectra of Ru/TASC (7 s interval). (**b**) Reaction equation for the reduction of 4-nitroaniline. (**c**) Reduction of 4-nitroaniline by ammonia borane by various ruthenium-impregnated catalysts. (**d**) log/log plot of rate vs concentration corresponding to the samples in panel **c**; the dashed line represents a first-order reaction.

Table 2. Overview of activity of catalysts for the reduction of 4-nitroaniline using ammonia borane.

#	Catalyst	Temperature [°C]	TOF[a] [mol_{4NA}/mol_{cat}, min^{-1}]	Ref.
1	$Ag_{0.64}$-$Au_{0.36}$@CeO_2	25	1.25	[60]
2	Pt/CeO_2-rGO	25	1.44	[61]
3	CoN@PCN	30	2.5	[62]
4	Ag/MTA	25	4.2[b]	[63]
5	$Au_{66}Pd_{34}$/C	25	4.8	[38]
6	Ru/TASC-NaOH	25	7.1	this work
7	$Cu_{0.8}Ni_{0.2}$-CeO_2/rGO	25	8.1	[64]
8	Ru/TASC-NaOH	45	13	this work
9	NP-Cu@Cu_2O	30	13	[65]
10	Pd@MIL-101	25	97	[66]

[a] Calculated using equation S1 in the supporting information. [b] $NaBH_4$ was used as a reductant.

the OH* intermediate combines with NH_3BH_2*, forming NH_3BH_2(OH)*, which then desorbs. The remaining B–H bonds react in a similar way. To check whether H_2 was an important intermediate in the reaction, we ran a control reaction using a H_2 as the sole reductant. After a 30 min induction period, the 4-nitroaniline slowly started converting at a rate of 0.077 h^{-1}, about 20.000 times slower than the reaction using ammonia borane as the reductant. Thus, hydrogen is not a main intermediate in this reaction.

To study the ruthenium nanoparticles, we used X-ray photoelectron spectroscopy (Figure S3–S6). The Ru 3d signal was convoluted with the C 1s signal so we had to establish some guidelines before we could properly deconvolute the signals. From control experiments on oxidized MAX phase and MXene (Figure S8) we observed a large signal at 284.8 (C–C) and a separate signal at 288 eV (COOH) with no large signals in between. Additionally, there were no large or distinct signals below 283 eV. Note that for HF-exfoliated MXene we *do* observe these signals corresponding to C–Ti–F group, but they are absent when using NaOH treatment. This means that the signals observed below 283 eV can only come from Ru $3d_{5/2}$. These signals are commonly found in the range 279.5–282.5 eV, depending on the oxidation state of ruthenium.[85,86] We also see a signal at 286.4 eV, which fits to Ru $3d_{3/2}$ signal with a spin-orbit splitting of 4.2 eV.[87,88] All samples show two distinct Ru signals: Ru(0) at 279.8 eV and Ru(IV) at 282.3 eV. This suggests that some of the Ru is in non-metallic form. A control experiment of ammonia borane hydrolysis using RuO_2 gave zero conversion, showing that the Ru(IV) species is inactive. Surprisingly for the most active catalyst, NaOH-treated MAX phase, the Ru(0) binding energy was decreased by 0.9 eV compared to Ru(0) on TASC MAX phase or $Ti_3C_2T_x$-HF. This shift, which indicates a higher electron density, reflects the high activity in ammonia borane hydrolysis.

Previously, we showed that electron-deficient Pt improves the activity of the metal for ammonia borane hydrolysis.[40] There the MXene formed a thin titania layer on the MXene surface, shifting the Pt to a higher binding energy. Here an opposite shift occurs. There are three differences that set the Ru results apart from the Pt ones. Firstly, Sn at the surface can interact with the Ru. Secondly, the support material is different. NaOH treatment does not leave any F groups on the MXene surface, which could react to form TiO_2. This means the Ru metal is in direct contact with the MXene, facilitating electron transfer. And finally, Ru is less electron-rich than Pt, so donating electrons to it could speed up the reaction.

Characterizing the electronic structure of the Ti is complicated by the overlap between the Ti 2p and Ru 3p signals. However, these signals can be extracted using a similar approach as with Ru 3d and C 1s. Ru 3p are much broader than Ti 2p and there are no Ru signals below 461 eV.[88–91] This means that the Ti 2p signals up to 459 eV can be quantitatively assigned. We observed Ti–C at 454.9 eV, Ti^{3+} at 457.1 eV and Ti^{4+} at 459.0 eV in all three samples (Figure 6d–f). After taking into consideration the spin-orbit splitting of 5.5 eV and a peak broadening of about 1.1–1.3 FWHM due to the Coster-Kronig effect,[92] we could extrapolate the Ti $2p_{1/2}$ peaks and estimate the broad Ru 3p signals (grey area in Figure 6d-f).

XPS shows an increase in Ti^{3+} level in the NaOH-treated sample, making it the predominant titanium species on the surface. This comes at the expense of the Ti–C species. Ti^{3+} species in TiO_2 are commonly associated with defects within TiO_2 defects.[93] Such high levels of Ti^{3+} might cause the strong downshift in Ru(0) on the NaOH-treated MXene. There is a correlation between TOF and Ti^{3+} concentration for the samples in the order TASC > $Ti_3C_2T_x$ > NaOH-treated TASC. The Ti^{3+} alone is not responsible for the catalytic effect, as no reaction occurs without ruthenium. Instead, we think that the electron-rich Ru(0) is influenced by Sn. Ru is present in two oxidation states: Ru(IV) and Ru(0). The Ru(0) signal was convoluted with many other signals, making it difficult to pinpoint the location of the Ru(IV) peak, and the quantity. Experiments using bulk RuO_2 as catalyst did not show any significant activity, suggesting that only Ru(0) contributes to the catalytic activity. Sn can form alloys or interact with ruthenium.[94–97] Tin can modify the selectivity of Ru in hydrogenation reactions.[96,98–101] It also stabilizes supported metals.[102] Our TASC-NaOH catalyst contains twice the amount of Sn on the surface compared to pristine TASC (Table 1, *cf.* entries 1/2). At low Ru concentrations and reduction at 350 °C, this may form an alloy.[103] When Sn and Ru are adjacent, Sn can donate electron-density to the Ru(0), explaining the downshift of 0.9 eV in XPS. The Ru nanoparticles are also very close to one another, enhancing this effect further. This also explains why the signal corresponding to RuO_x is not shifted as much as Ru(0); this species is electron-deficient and non-conductive, making an interaction with Ti–C

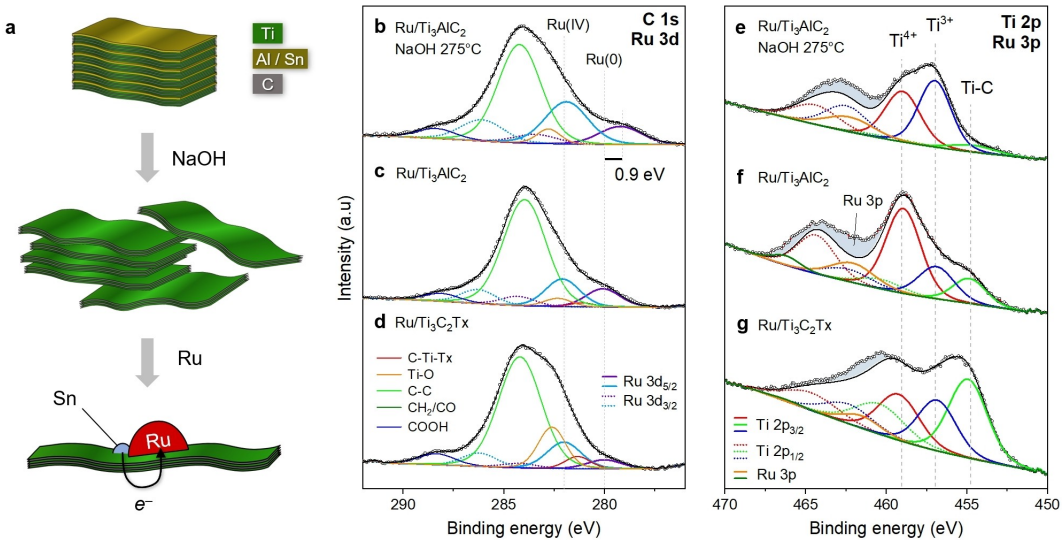

Figure 6. (**a**) Cartoon of the TASC synthesis and the interaction between Ru and Sn. C 1s XPS spectra of (**b**) Ru/NaOH-treated TASC MAX phase, (**c**) Ru/TASC MAX phase and (**d**) Ru/Ti_3C_2Tx MXene. Ti 2p XPS spectra of (**e**) Ru/NaOH-treated TASC MAX phase, (**f**) Ru/TASC MAX phase and (**g**) Ru/Ti_3C_2Tx MXene. The grey area in **e**–**g** represents the Ru 3p signal.

or the neighbouring Ru(0) difficult. XPS analysis reveals that Ru^{4+} is present on the surface, indicating that the samples were likely oxidized after the reduction treatment. This RuO_x layer is likely responsible for the small induction period (< 2 min) before full catalytic activity is observed (Figure S12, left, Ru/TASC-NaOH). Likely, this RuO_x is reduced *in situ* by the ammonia borane at the start of the reaction. Direct reduction of the Ru-impregnated supports (before heat treatment and reduction) using ammonia borane was unsuccessful because Ru leached out before it could be reduced. This makes the heat treatment and H_2 reduction steps essential to ensure proper binding of Ru to the support.

To rule out any negative influence of Cl^- or Na^+, we conducted an experiment with 0.4% Ru/TASC-NaOH where we injected a solution of NaCl (0.4 mL, 2 M) when an isothermal reaction at 30 °C reached 10% conversion. The Hydrogen production rate was practically unaffected and decreased by < 0.3% after NaCl addition.

Conclusion

We successfully synthesized a disordered MAX phase, TASC, with ribbon-like structures using a method utilizing dilute NaOH whilst avoiding side-reactions producing NTOs. The surface of this material contains Sn and Ti^{3+}, both of which can interact with ruthenium, decreasing the electron binding energy of the metallic Ru. This shift in binding energy is likely responsible for the high activity in ammonia borane hydrolysis giving a TOF of 582 min^{-1} at 30 °C using a loading of only 0.4 wt% ruthenium. Our work shows that MAX phases and their modified derivatives offer plenty of opportunities to design catalysts with more desirable catalytic properties.

Experimental Section

An extensive description of experimental details is provided in the supporting information.

TASC MAX phase synthesis

A mixture of titanium, aluminium, tin and TiC powder (in the atomic ratio 1:1:0.2:1.9) was mixed with a stainless-steel milling ball for 24 h. The powder mixture was heated at 1450 °C for 15 min in Ar. Once the mixture was cooled down to room temperature, the resulting Ti_3AlC_2 was crushed and milled into the required powders. This material has the composition $Ti_3(Al_{0.8}Sn_{0.2})C_2$ and is denoted as TASC.

MXene synthesis

Procedure for delamination using hydrogen fluoride

Ti_3AlC_2 was etched with HF for 7 days under continuous ultra-sonication. The mixture was washed with deionized water (15x) until the pH of the mixture was neutral and dried under vacuum. This material is denoted as Ti_3C_2Tx.

Procedure for etching using sodium hydroxide treatment

$Ti_3(Al_{0.8}Sn_{0.2})C_2$ (1.0 g) was loaded in a 75 mL autoclave and 4 M NaOH solution (25 mL) was added. The autoclave was immediately sealed after addition. The mixture was stirred and heated at 200 °C, 275 °C, or 350 °C for 20 hours. The autoclave was cooled to room temperature. The remaining solid material was collected, washed with H_2O (10x) and ethanol (2x), then dried under vacuum at 30 °C.

Impregnation procedure

The impregnation procedure has been adapted from the well-known double-solvent method.[36] The support material (100 mg) was loaded into a 2 mL vial with 1 mL of hexanes. Ruthenium

chloride hydrate (99.9%, STREM, lot 30437800), $RuCl_3{\cdot}xH_2O$, (30.3 mg, assay: 43.1% Ru metal content) was dissolved in water (1 mL) and 40 μL of this solution was added to the material suspension and stirred overnight. The suspension was decanted and the solid was dried in air for 3 h. The impregnated materials were further dried at 80 °C for 3 h, 120 °C for 2 h and then heat-treated in nitrogen at 350 °C for 1 h. The resulting samples were then reduced at 350 °C for 1 h in a 250 mL/min stream of 10% hydrogen in nitrogen. The temperature of 350 °C was chosen to fully reduce Ru and enable Ru–Sn alloy formation.

General procedure for ammonia borane hydrolysis

A 10 mL reactor was loaded with catalyst (2.0 mg), water (8 mL), and an 8×3 mm stirrer bar. The reactor was then cooled to around 20 °C on an ice bath after purging with H_2 for 5 min. Ammonia borane (2 M, 400 μL) was injected into the reactor through a glass capillary directly into the solution and the sample was stirred continuously at 600 rpm. The sample was heated at a ramp rate of 2 °C min^{-1} to 85 °C and held there until no more gas evolved from the reaction. Hydrogen production was monitored throughout the experiment by counting bubbles which form in a hexadecane medium.[37] A blank experiment with only water (8.4 mL) was also performed to record the background gas expansion and increasing vapour pressure of the solvent. This blank was subtracted from all experiments.

For the experiments in the presence of NaCl, a similar procedure was used. An additional syringe with NaCl solution (0.4 mL, 2 M) was attached to the reactor, and was injected when the reaction reached about 10% conversion. The gas production rate was monitored before and after injection of the NaCl. A linear fit to the volume (corresponding to ~1 mL H_2 gas) before and after addition yielded the gas production rates before and after the NaCl addition.

General procedure for reduction of 4-nitroaniline

A standard quartz UV/Vis cuvette (l = 1 cm) was loaded with catalyst (0.20 mg), water (2 mL) and a small stirrer bar. Ammonia borane (1 M, 10 μL) was added to the cuvette and the reaction mixture was stirred (1000 rpm) for 5 min. Then, an aqueous solution of 4-nitroaniline (5 mM, 50 μL) was added, marking the start of the reaction. The reaction mixture was stirred constantly (1000 rpm) while obtaining UV/Vis spectra in the range of 700–190 nm every 6–8 s.

Acknowledgements

We thank ing. N.J. Geels and Dr. A. Gheorghe for help with the N_2 adsorption experiments. T.K.S. was supported by NWO TOP-PUNT grant 718.015.004. P.O. thanks the Spanish Ministry of Science, Innovation and Universities (Project MCIU-19-RTI2018-094218-B–I00), and acknowledges the technical support provided by Scientific and Technical Services of the University of Oviedo and the Advanced Microscopy Laboratory. Z.S. was supported by Czech Science Foundation (GACR No. 20-16124 J).

Conflict of Interest

The authors declare no conflict of interest.

Keywords: disordered MAX phase · heterogeneous catalysis · ruthenium · metal-support interaction · hydrogenation

[1] M. Naguib, M. Kurtoglu, V. Presser, J. Lu, J. Niu, M. Heon, L. Hultman, Y. Gogotsi, M. W. Barsoum, *Adv. Mater.* **2011**, *23*, 4248–4253.
[2] W. H. K. Ng, E. S. Gnanakumar, E. Batyrev, S. K. Sharma, P. K. Pujari, H. F. Greer, W. Zhou, R. Sakidja, G. Rothenberg, M. W. Barsoum, N. R. Shiju, *Angew. Chem. Int. Ed.* **2018**, *57*, 1485–1490; *Angew. Chem.* **2018**, *130*, 1501–1506.
[3] M. Ronda-Lloret, V. S. Marakatti, W. G. Sloof, J. J. Delgado, A. Sepúlveda-Escribano, E. V. Ramos-Fernandez, G. Rothenberg, N. R. Shiju, *ChemSusChem* **2020**, *13*, 6401–6408.
[4] M. Naguib, V. N. Mochalin, M. W. Barsoum, Y. Gogotsi, *Adv. Mater.* **2014**, *26*, 992–1005.
[5] M. W. Barsoum, MAX Phases: Properties of Machinable Ternary Carbides and Nitrides, John Wiley & Sons, **2013**.
[6] J. L. Hart, K. Hantanasirisakul, A. C. Lang, B. Anasori, D. Pinto, Y. Pivak, J. T. van Omme, S. J. May, Y. Gogotsi, M. L. Taheri, *Nat. Commun.* **2019**, *10*, 522.
[7] G. Gao, A. P. O'Mullane, A. Du, *ACS Catal.* **2017**, *7*, 494–500.
[8] J. Halim, I. Persson, E. J. Moon, P. Kühne, V. Darakchieva, P. O. Å. Persson, P. Eklund, J. Rosen, M. W. Barsoum, *J. Phys. Condens. Matter* **2019**, *31*, 165301.
[9] A. Miranda, J. Halim, M. W. Barsoum, A. Lorke, *Appl. Phys. Lett.* **2016**, *108*, 033102.
[10] S. Zhou, X. Yang, W. Pei, N. Liu, Jijun. Zhao, *Nanoscale* **2018**, *10*, 10876–10883.
[11] Y. Jiang, T. Sun, X. Xie, W. Jiang, J. Li, B. Tian, C. Su, *ChemSusChem* **2019**, *12*, 1368–1373.
[12] J. Zhang, Y. Zhao, X. Guo, C. Chen, C.-L. Dong, R.-S. Liu, C.-P. Han, Y. Li, Y. Gogotsi, G. Wang, *Nat. Catal.* **2018**, *1*, 985–992.
[13] Z. Li, L. Yu, C. Milligan, T. Ma, L. Zhou, Y. Cui, Z. Qi, N. Libretto, B. Xu, J. Luo, E. Shi, Z. Wu, H. Xin, W. N. Delgass, J. T. Miller, Y. Wu, *Nat. Commun.* **2018**, *9*, 1–8.
[14] A. Feng, Y. Yu, Y. Wang, F. Jiang, Y. Yu, L. Mi, L. Song, *Mater. Des.* **2017**, *114*, 161–166.
[15] M. Naguib, R. R. Unocic, B. L. Armstrong, J. Nanda, *Dalton Trans.* **2015**, *44*, 9353–9358.
[16] G. Lv, J. Wang, Z. Shi, L. Fan, *Mater. Lett.* **2018**, *219*, 45–50.
[17] O. Mashtalir, M. Naguib, V. N. Mochalin, Y. Dall'Agnese, M. Heon, M. W. Barsoum, Y. Gogotsi, *Nat. Commun.* **2013**, *4*, 1716.
[18] A. Qian, J. Y. Seo, H. Shi, J. Y. Lee, C.-H. Chung, *ChemSusChem* **2018**, *11*, 3719–3723.
[19] S. Elumalai, M. Yoshimura, M. Ogawa, *Chem. Asian J.* **2020**, *15*, 1044–1051.
[20] Y. Chae, S. Joon Kim, S.-Y. Cho, J. Choi, K. Maleski, B.-J. Lee, H.-T. Jung, Y. Gogotsi, Y. Lee, C. Won Ahn, *Nanoscale* **2019**, *11*, 8387–8393.
[21] H. Tang, S. Zhuang, Z. Bao, C. Lao, Y. Mei, *ChemElectroChem* **2016**, *3*, 871–876.
[22] M. Cao, F. Wang, L. Wang, W. Wu, W. Lv, J. Zhu, *J. Electrochem. Soc.* **2017**, *164*, A3933.
[23] R. Lotfi, M. Naguib, D. E. Yilmaz, J. Nanda, A. C. T. van Duin, *J. Mater. Chem. A* **2018**, *6*, 12733–12743.
[24] T. Li, L. Yao, Q. Liu, J. Gu, R. Luo, J. Li, X. Yan, W. Wang, P. Liu, B. Chen, W. Zhang, W. Abbas, R. Naz, D. Zhang, *Angew. Chem. Int. Ed.* **2018**, *57*, 6115–6119; *Angew. Chem.* **2018**, *130*, 6223–6227.
[25] P. Gu, S. Zhang, C. Zhang, X. Wang, A. Khan, T. Wen, B. Hu, A. Alsaedi, T. Hayat, X. Wang, *Dalton Trans.* **2019**, *48*, 2100–2107.
[26] X. Xie, Y. Xue, L. Li, S. Chen, Y. Nie, W. Ding, Z. Wei, *Nanoscale* **2014**, *6*, 11035–11040.
[27] D. Sun, A. Zhou, Z. Li, L. Wang, *J. Adv. Ceram.* **2013**, *2*, 313–317.
[28] D. Li, Y. Liang, X. Liu, Y. Zhou, *J. Eur. Ceram. Soc.* **2010**, *30*, 3227–3234.
[29] J. Xuan, Z. Wang, Y. Chen, D. Liang, L. Cheng, X. Yang, Z. Liu, R. Ma, T. Sasaki, F. Geng, *Angew. Chem. Int. Ed.* **2016**, *55*, 14569–14574; *Angew. Chem.* **2016**, *128*, 14789–14794.
[30] C. Zeng, F. Xie, X. Yang, M. Jaroniec, L. Zhang, S.-Z. Qiao, *Angew. Chem.* **2018**, *130*, 8676–8680; *Angew. Chem. Int. Ed.* **2018**, *57*, 8540–8544.
[31] X. Sun, K. Tan, Y. Liu, J. Zhang, L. Hou, C. Yuan, *Chin. Chem. Lett.* **2020**, *31*, 2254–2258.
[32] Z. Wei, Z. Peigen, T. Wubian, Q. Xia, Z. Yamei, S. ZhengMing, *Mater. Chem. Phys.* **2018**, *206*, 270–276.
[33] Y. Dong, Z.-S. Wu, S. Zheng, X. Wang, J. Qin, S. Wang, X. Shi, X. Bao, *ACS Nano* **2017**, *11*, 4792–4800.

[34] Q. Xu, J. Xu, H. Jia, Q. Tian, P. Liu, S. Chen, Y. Cai, X. Lu, X. Duan, L. Lu, *J. Electroanal. Chem.* **2020**, *860*, 113869.
[35] Z. Li, Y. Cui, Z. Wu, C. Milligan, L. Zhou, G. Mitchell, B. Xu, E. Shi, J. T. Miller, F. H. Ribeiro, Y. Wu, *Nat. Catal.* **2018**, *1*, 349–355.
[36] A. Aijaz, A. Karkamkar, Y. J. Choi, N. Tsumori, E. Rönnebro, T. Autrey, H. Shioyama, Q. Xu, *J. Am. Chem. Soc.* **2012**, *134*, 13926–13929.
[37] T. K. Slot, N. R. Shiju, G. Rothenberg, *Angew. Chem. Int. Ed.* **2019**, *58*, 17273–17276; *Angew. Chem.* **2019**, *131*, 17433–17436.
[38] M. Muzzio, H. Lin, K. Wei, X. Guo, C. Yu, T. Yom, Z. Xi, Z. Yin, S. Sun, *ACS Sustainable Chem. Eng.* **2020**, *8*, 2814–2821.
[39] Y.-H. Zhou, Q. Yang, Y.-Z. Chen, H.-L. Jiang, *Chem. Commun.* **2017**, *53*, 12361–12364.
[40] T. K. Slot, F. Yue, H. Xu, E. V. Ramos-Fernandez, A. Sepúlveda-Escribano, Z. Sofer, G. Rothenberg, N. R. Shiju, *2D Mater.* **2020**, *8*, DOI 10.1088/2053-1583/ababef.
[41] V. Natu, J. L. Hart, M. Sokol, H. Chiang, M. L. Taheri, M. W. Barsoum, *Angew. Chem. Int. Ed.* **2019**, *58*, 12655–12660; *Angew. Chem.* **2019**, *131*, 12785–12790.
[42] R. Zheng, C. Shu, Z. Hou, A. Hu, P. Hei, T. Yang, J. Li, R. Liang, J. Long, *ACS Appl. Mater. Interfaces* **2019**, *11*, 46696–46704.
[43] C. Magnus, D. Cooper, J. Sharp, W. M. Rainforth, *Wear* **2019**, *438–439*, 203013.
[44] S. Rico-Francés, E. O. Jardim, T. A. Wezendonk, F. Kapteijn, J. Gascon, A. Sepúlveda-Escribano, E. V. Ramos-Fernandez, *Appl. Catal. B* **2016**, *180*, 169–178.
[45] T. Mazza, E. Barborini, P. Piseri, P. Milani, D. Cattaneo, A. Li Bassi, C. E. Bottani, C. Ducati, *Phys. Rev. B* **2007**, *75*, 045416.
[46] Y. Zhang, W. Wu, K. Zhang, C. Liu, A. Yu, M. Peng, J. Zhai, *Phys. Chem. Chem. Phys.* **2016**, *18*, 32178–32184.
[47] R. Wang, Y. Wang, M. Ren, G. Sun, D. Gao, Y. R. Chin Chong, X. Li, G. Chen, *Int. J. Hydrogen Energy* **2017**, *42*, 6757–6764.
[48] S. Akbayrak, Y. Tonbul, S. Özkar, *Dalton Trans.* **2016**, *45*, 10969–10978.
[49] Y. Fan, X. Li, X. He, C. Zeng, G. Fan, Q. Liu, D. Tang, *Int. J. Hydrogen Energy* **2014**, *39*, 19982–19989.
[50] Y. Tonbul, S. Akbayrak, S. Özkar, *J. Colloid Interface Sci.* **2018**, *513*, 287–294.
[51] S. Akbayrak, G. Çakmak, T. Öztürk, S. Özkar, *Int. J. Hydrogen Energy* **2021**, *46*, 13548–13560.
[52] K. Mori, K. Miyawaki, H. Yamashita, *ACS Catal.* **2016**, *6*, 3128–3135.
[53] S. Akbayrak, S. Özkar, *ACS Appl. Mater. Interfaces* **2012**, *4*, 6302–6310.
[54] E. B. Kalkan, S. Akbayrak, S. Özkar, *J. Mol. Catal.* **2017**, *430*, 29–35.
[55] E. Taşçı, S. Akbayrak, S. Özkar, *Int. J. Hydrogen Energy* **2018**, *43*, 15124–15134.
[56] C. Du, Q. Ao, N. Cao, L. Yang, W. Luo, G. Cheng, *Int. J. Hydrogen Energy* **2015**, *40*, 6180–6187.
[57] Y. He, Y. Peng, Y. Wang, Y. Long, G. Fan, *Fuel* **2021**, *297*, 120750.
[58] Y. Peng, Y. He, Y. Wang, Y. Long, G. Fan, *J. Colloid Interface Sci.* **2021**, *594*, 131–140.
[59] F. Fu, C. Wang, Q. Wang, A. M. Martinez-Villacorta, A. Escobar, H. Chong, X. Wang, S. Moya, L. Salmon, E. Fouquet, J. Ruiz, D. Astruc, *J. Am. Chem. Soc.* **2018**, *140*, 10034–10042.
[60] D. Liu, W. Li, X. Feng, Y. Zhang, *Chem. Sci.* **2015**, *6*, 7015–7019.
[61] X. Wang, D. Liu, S. Song, H. Zhang, *J. Am. Chem. Soc.* **2013**, *135*, 15864–15872.
[62] L. Zhang, J. Wang, N. Shang, S. Gao, Y. Gao, C. Wang, *Appl. Surf. Sci.* **2019**, *491*, 544–552.
[63] D. Andreou, D. Iordanidou, I. Tamiolakis, G. S. Armatas, I. N. Lykakis, *Nanomaterials* **2016**, *6*, 54.
[64] Y.-H. Zhou, S. Wang, Y. Wan, J. Liang, Y. Chen, S. Luo, C. Yong, *J. Alloys Compd.* **2017**, *728*, 902–909.
[65] J. Du, J. Hou, B. Li, R. Qin, C. Xu, H. Liu, *J. Alloys Compd.* **2020**, *815*, 152372.
[66] Q. Yang, Y.-Z. Chen, Z. U. Wang, Q. Xu, H.-L. Jiang, *Chem. Commun.* **2015**, *51*, 10419–10422.
[67] S. Ghosh, B. R. Jagirdar, *Dalton Trans.* **2018**, *47*, 17401–17411.
[68] J. Du, J. Chen, H. Xia, Y. Zhao, F. Wang, H. Liu, W. Zhou, B. Wang, *ChemCatChem* **2020**, *12*, 2426–2430.
[69] X. Li, L. Song, D. Gao, B. Kang, H. Zhao, C. Li, X. Hu, G. Chen, *Chem. Eur. J.* **2020**, *26*, 4419–4424.
[70] Q. Sun, N. Wang, T. Zhang, R. Bai, A. Mayoral, P. Zhang, Q. Zhang, O. Terasaki, J. Yu, *Angew. Chem. Int. Ed.* **2019**, *58*, 18570–18576; *Angew. Chem.* **2019**, *131*, 18743–18749.
[71] Ö. Metin, A. Mendoza-Garcia, D. Dalmızrak, M. S. Gültekin, S. Sun, *Catal. Sci. Technol.* **2016**, *6*, 6137–6143.
[72] K. Ganjehyan, B. Nişancı, M. Sevim, A. Daştan, Ö. Metin, *Appl. Organomet. Chem.* **2019**, *33*, e4863.
[73] X. Liu, L. Zhang, J. Wang, N. Shang, S. Gao, C. Wang, Y. Gao, *Appl. Organomet. Chem.* **2020**, *34*, e5438.
[74] S. N. H. MD Dostagir, M. K. Awasthi, A. Kumar, K. Gupta, S. Behrens, A. Shrotri, S. K. Singh, *ACS Sustainable Chem. Eng.* **2019**, *7*, 9352–9359.
[75] W. Chen, D. Li, Z. Wang, G. Qian, Z. Sui, X. Duan, X. Zhou, I. Yeboah, D. Chen, *AIChE J.* **2017**, *63*, 60–65.
[76] T. K. Slot, N. Riley, N. R. Shiju, J. W. Medlin, G. Rothenberg, *Chem. Sci.* **2020**, *11*, 11024–11029.
[77] K. Feng, J. Zhong, B. Zhao, H. Zhang, L. Xu, X. Sun, S.-T. Lee, *Angew. Chem. Int. Ed.* **2016**, *55*, 11950–11954; *Angew. Chem.* **2016**, *128*, 12129–12133.
[78] Q. Wang, F. Fu, S. Yang, M. Martinez Moro, M. de los A. Ramirez, S. Moya, L. Salmon, J. Ruiz, D. Astruc, *ACS Catal.* **2019**, *9*, 1110–1119.
[79] F. Fu, C. Wang, Q. Wang, A. M. Martinez-Villacorta, A. Escobar, H. Chong, X. Wang, S. Moya, L. Salmon, E. Fouquet, J. Ruiz, D. Astruc, *J. Am. Chem. Soc.* **2018**, *140*, 10034–10042.
[80] H. Wu, Q. Luo, R. Zhang, W. Zhang, J. Yang, *Chin. J. Chem. Phys.* **2018**, *31*, 641–648.
[81] L. Wang, H. Li, W. Zhang, X. Zhao, J. Qiu, A. Li, X. Zheng, Z. Hu, R. Si, J. Zeng, *Angew. Chem. Int. Ed.* **2017**, *56*, 4712–4718; *Angew. Chem.* **2017**, *129*, 4790–4796.
[82] T. Banu, T. Debnath, T. Ash, A. K. Das, *J. Chem. Phys.* **2015**, *143*, 194305.
[83] L.-L. Long, X.-Y. Liu, J.-J. Chen, J. Jiang, C. Qian, G.-X. Huang, Q. Rong, X. Zhang, H.-Q. Yu, *ACS Appl. Nano Mater.* **2018**, *1*, 6800–6807.
[84] Y. Li, M. Hu, J. Wang, W.-H. Wang, *J. Organomet. Chem.* **2019**, *899*, 120913.
[85] D. J. Morgan, *Surf. Interface Anal.* **2015**, *47*, 1072–1079.
[86] J. Balcerzak, W. Redzynia, J. Tyczkowski, *Appl. Surf. Sci.* **2017**, *426*, 852–855.
[87] L.-Å. Näslund, Á. S. Ingason, S. Holmin, J. Rosen, *J. Phys. Chem. C* **2014**, *118*, 15315–15323.
[88] P. Paunović, D. S. Gogovska, O. Popovski, A. Stoyanova, E. Slavcheva, E. Lefterova, P. Iliev, A. T. Dimitrov, S. H. Jordanov, *Int. J. Hydrogen Energy* **2011**, *36*, 9405–9414.
[89] J. Wojciechowska, E. Gitzhofer, J. Grams, A. Ruppert, N. Keller, *Materials* **2018**, *11*, 2329.
[90] H. Cheng, W. Lin, X. Li, C. Zhang, F. Zhao, *Catalysts* **2014**, *4*, 276–288.
[91] B. Coşkuner Filiz, E. S. Gnanakumar, A. Martínez-Arias, R. Gengler, P. Rudolf, G. Rothenberg, N. R. Shiju, *Catal. Lett.* **2017**, *147*, 1744–1753.
[92] M. Ohno, *J. Electron Spectrosc. Relat. Phenom.* **2004**, *136*, 221–228.
[93] M. J. Jackman, A. G. Thomas, C. Muryn, *J. Phys. Chem. C* **2015**, *119*, 13682–13690.
[94] M. J. Mendes, O. A. A. Santos, E. Jordão, A. M. Silva, *Appl. Catal. Gen.* **2001**, *217*, 253–262.
[95] L. Perring, P. Feschotte, F. Bussy, J. C. Gachon, *J. Alloys Compd.* **1996**, *245*, 157–163.
[96] E. Bonnefille, F. Novio, T. Gutmann, R. Poteau, P. Lecante, J.-C. Jumas, K. Philippot, B. Chaudret, *Nanoscale* **2014**, *6*, 9806–9816.
[97] L. Stievano, S. Calogero, F. E. Wagner, S. Galvagno, C. Milone, *J. Phys. Chem. B* **1999**, *103*, 9545–9556.
[98] K. Y. Cheah, T. S. Tang, F. Mizukami, S. Niwa, M. Toba, Y. M. Choo, *J. Am. Oil Chem. Soc.* **1992**, *69*, 410–416.
[99] M. Toba, S. Tanaka, S. Niwa, F. Mizukami, Z. Koppány, L. Guczi, K.-Y. Cheah, T.-S. Tang, *Appl. Catal. Gen.* **1999**, *189*, 243–250.
[100] V. M. Deshpande, K. Ramnarayan, C. S. Narasimhan, *J. Catal.* **1990**, *121*, 174–182.
[101] K. Tahara, E. Nagahara, Y. Itoi, S. Nishiyama, S. Tsuruya, M. Masai, *J. Mol. Catal. Chem.* **1996**, *110*, L5–L6.
[102] Y. Hara, K. Endou, *Appl. Catal. Gen.* **2003**, *239*, 181–195.
[103] V. A. Mazzieri, M. R. Sad, C. R. Vera, C. L. Pieck, R. Grau, *Quim. Nova* **2010**, *33*, 269–272.

Manuscript received: January 29, 2021
Revised manuscript received: May 11, 2021
Accepted manuscript online: May 16, 2021
Version of record online: June 24, 2021